

A NEW ANALYTICAL METHOD FOR CHARACTERIZATION OF  
FRACTURED RESERVOIRS

ZOHREH MOVAHED

A thesis submitted in fulfilment of the  
requirements for the award of the degree of  
Doctor of Philosophy (Petroleum Engineering)

Faculty of Petroleum and Renewable Energy Engineering  
Universiti Teknologi Malaysia

SEPTEMBER 2015

Specially dedicated to *my mother*

I really miss you

*Al-Fatihah*

## ACKNOWLEDGEMENT

I owe the accomplishment of the whole work to all precious figures who grant me their kindest inspirations and contributions, to begin with Universiti Teknologi Malaysia (UTM) for great services and kindest support of academic and non-academic staff, my dear supervisor, Professor Dr. Radzuan Junin, the scholarly mentor who had a fundamental role to lead me on all paths to reach success point, put his all attempts in guiding the team to achieve our scientific goals and prominent research publications, to allow me to grow as a research scientist and the approval of the thesis for defense. I would like to express the deepest appreciation to my industrial supervisor Dr. Hassan Amiri Bakhtiary, who has the attitude as a genius in the field of this study. He granted me the permission to have access and use all required data and the necessary materials to accomplish the work. I pay my heartiest tribute to the committee members to contribute us on all processes and steps to early submit and defense of the work along with amity and goodwill of the Faculty of Petroleum and Renewable Energy Engineering during all these precious years.

I highly appreciate the guidance given by other supervisors as well as the panels, especially in our project that has improved our work skills; thanks to their comment and advices. I would like to thank Mostafa Alizadeh, who have assisted me in inserting format revisions and I required to be carried out into the researches. I would also like to thank all of my friends in NIOC south specially Mrs. Ruhangiz Mohamadian who supported me in getting the data, and incited me to strive towards my goal. A special thanks to my family. Words cannot express how grateful I am with my lovely mother, father, sisters and brothers for all of the sacrifices that you've made on my behalf. Your prayer for me was what sustained me thus far. Although, my lovely mother passed away without having any disease during my study here in Malaysia, and it was bad shocked for me, but her advises and prayers have been great sources of motivation and I recovered from this loss and strived to finish this study to make her soul happy. At the end, I would like to express appreciation to my beloved husband Ahmad, who spent sleepless nights with and he was always my support in difficulties and the moments when there was no one to answer my queries and my respect to the beautiful Malaysia to provide any needs and excellent unique public facilities and its kindest people in the world.

## ABSTRACT

Structural delineation is the main issue in the evaluation of carbonate reservoirs in structurally complex areas. Permeability is a critical reservoir parameter that influences well and/or reservoir performance and it is even more challenging when the reservoir is fractured. Oil Based Mud Micro Imager - resistivity of invading zone (OBMI-Rxo) is a high resolution curve that is sensitive to fluid mobility near the borehole wall and indicates invasion. However most operators are not using an accurate Rxo curve of OBMI for reservoir and petrophysical applications. After drilling it is important that the borehole stays in good shape, moreover, borehole instability will reduce the working life of the well. The main aim of this study is to design a workflow in order to establish an advanced formation evaluation in a carbonate fractured and clastic reservoirs. The entire workflow involved incorporating borehole images, petrophysical logs, Modular Formation Dynamics Tester tool (MDT), Xpress Pressure Tool (XPT) and cores in characterizing fractured and non-fractured reservoirs. Image log data are processed and interpreted in the computer using a Geoframe software. The bedding, deviation survey and image logs are imported into the Bortex software and the heterogeneity analysis of reservoirs from borehole images is computed based on the same resistivity contrast principle than the layer delineation. Respectively, the Formation Micro Imager (FMI) and OBMI images are used to examine permeability and index mobility in conjunction with open hole logs. As a result, the answers provided by the FMI tool helped in understanding the reservoir structure, identify and evaluate fractures, visualize the rock texture, and complement coring programs. Single-well permeability distribution was demonstrated by the use of advanced image analysis. OBMI-Rxo helped to identify zones of higher permeability when combined with conventional induction logs and porosity logs. In addition, working on advanced borehole shape analysis improved information about the well condition.

## ABSTRAK

Struktur delineasi menjadi isu yang utama untuk penilaian reservoir karbonat di kawasan berstruktur rencam. Ketertelapan merupakan parameter reservoir kritikal yang dapat mempengaruhi pelakuan telaga dan/atau reservoir dan ianya didapati lebih mencabar apabila reservoir mempunyai rekahan. Pengimbas Mikro Lumpur Dasar Minyak – kerintangan zon serbuan (OBMI-Rxo) adalah lengkuk beresolusi tinggi yang sensitif kepada pergerakan bendalir berhampiran dinding lubang telaga dan yang menunjukkan penyerbuan, kebanyakan operator didapati tidak menggunakan lengkuk OBMI-Rxo dengan betul pada reservoir dan bagi aplikasi petrofizik. Selepas penggerudian dijalankan, adalah penting untuk memastikan lubang telaga dalam bentuk yang baik. Tambahan pula, ketidakstabilan lubang telaga akan mengurangkan jangka hayat telaga tersebut. Tujuan utama kajian ini adalah untuk merekabentuk carta alir kerja tetap bagi penilaian formasi lanjutan untuk reservoir karbonat rekah dan juga klastik. Secara keseluruhannya, carta alir kerja ini untuk tujuan pencirian reservoir rekah dan bukan rekah adalah merangkupi imej lubang telaga, log petrofizik, ‘modular formation dynamics tester tool’, ‘Xpress pressure tool’ dan teras. Data log imej diproses dan diterjemah dengan menggunakan komputer dengan perisian ‘Geoframe’. Data dari lapisan, survei deviasi dan imej log diimport ke dalam perisian ‘Bortex’ dan kemudiannya pengiraan analisis keheterogenan reservoir daripada imej lubang telaga dilakukan berdasar kepada prinsip perbezaan kesamaan resistiviti berbanding deliniasi lapisan. Berkaitan log lubang telaga terbuka, pengimbas mikro formasi (FMI) diguna untuk menilai ketertelapan, manakala imej OBMI diguna untuk menilai indeks mobiliti. Sebagai kesimpulan, hasil yang diberi oleh alatan FMI didapati dapat membantu dalam penelitian struktur reservoir, mengecam dan menilai rekahan, memapar tekstur batuan, dan pelengkapan program penerasan. Taburan ketertelapan telaga tunggal telah dipapar dengan menggunakan analisis imej lanjutan. OBMI-Rxo membantu untuk mengenal zon ketertelapan tinggi apabila ianya digabungkan dengan log induksi konvensional dan log keliangan. Berkaitan kestabilan lubang telaga, kajian ini juga didapati dapat menambah baik maklumat tentang keadaan telaga apabila dijalankan analisis lanjutan bentuk lubang telaga.

## TABLE OF CONTENTS

CHAPTER	TITLE	PAGE
	<b>DECLARATION</b>	ii
	<b>DEDICATION</b>	iii
	<b>ACKNOWLEDGEMENT</b>	iv
	<b>ABSTRACT</b>	v
	<b>ABSTRAK</b>	vi
	<b>TABLE OF CONTENTS</b>	vii
	<b>LIST OF TABLES</b>	xii
	<b>LIST OF FIGURES</b>	xiii
	<b>LIST OF ABBREVIATIONS</b>	xxii
	<b>LIST OF SYMBOLS</b>	xxiv
 <b>1</b>	 <b>INTRODUCTION</b>	 <b>1</b>
	1.1 Introduction	1
	1.2 Problem Statement	4
	1.3 Objectives of the Research	5
	1.4 Scopes of the Research	5
 <b>2</b>	 <b>LITERATURE REVIEW</b>	 <b>7</b>
	2.1 Introduction	7
	2.2 Asmari Reservoir	8
	2.3 Sarvak Reservoir	8
	2.4 Structural Complexity in the Zagros and Studied Oil Fields	10
	2.4.1 Fault Types in Complex Reservoir	13
	2.5 Fractures in Complex Structures	14

2.6	Permeability in Fractured Carbonate Reservoir	16
2.7	Oil Based Mud System in Iran	18
2.8	Borehole Imaging Development and Application	19
2.9	Borehole Imaging Tools	23
2.9.1	Water Based Mud Imaging	23
2.9.2	Oil Based Mud Imaging	23
2.10	Summary	32
<b>3</b>	<b>RESEARCH METHODOLOGY</b>	<b>36</b>
3.1	Introduction	36
3.2	Data Collection	37
3.2.1	Geological data – FMI, OBMI-UBI and Cores	38
3.2.2	Petrophysical data – PEX, HRLA	40
3.2.3	Formation testing data – MDT and XPT	40
3.3	Data Quality	41
3.4	FMI Log Processing	43
3.4.1	Sticking Detection and Speed Correction	45
3.4.2	FMI Scaling	46
3.4.3	Static and Dynamic Normalization of FMI Image in BorNor	49
3.5	OBMI Log Processing	51
3.5.1	Sticking Detection and Speed Correction in BorEid	51
3.5.2	Static and Dynamic Normalization in BorNor	51
3.6	UBI Log Processing	52
3.7	FMI Log Interpretation	55
3.7.1	Dip Interpretation on Image Log in BorView as input to BorTex Module	59
3.7.2	BorTex	64
3.8	OBMI-UBI Log Interpretation	71
3.8.1	Bedding	71
3.8.2	Fractures	72

3.9	BorTex Processing for deriving SRES	75
3.10	Summary	77

## **4 RESERVOIR CHARACTERIZATION BY USING FMI, MDT AND CORES 79**

4.1	Introduction	79
4.2	An Accurate Structural Model by Introducing a Structural System in the Complex Fractured Reservoirs (LL-26)	81
4.2.1	Structural and Fracture Interpretation	81
4.2.2	Complex Fault System	84
4.3	Permeability Analysis in Asmari Reservoir (PZ-126)	90
4.3.1	Structural Dip as Input Data for Permeability Analysis in PZ-126	90
4.3.2	Natural Fracture Characterization (Verification Data)	96
4.4	Permeability Result	102
4.5	Porosity Result and Integration of Porosity and Permeability Result from FMI	104
4.6	Verification of FMI Permeability with MDT Permeability	106
4.7	Verification of FMI Permeability with Core Permeability in PZ-126	109
4.8	Verification of FMI Permeability with Core Permeability in Non-Highly Fractured Reservoir	110
4.9	The Effect of Tar on the Permeability Analysis from FMI in Asmari Fractured Reservoir (RS-55)	115
4.10	Summary	117

## **5 RESERVOIR CHARACTERIZATION BY USING OBMI, XPT AND CORES 119**

5.1	Introduction	119
5.2	Structural Dip as Input Data for Mobility Analysis	121
5.2.1	Zone 1	124
5.2.2	Zone 11	126



	5.2.3	Zone 20	127
	5.2.4	Sub Zone 28	128
	5.2.5	Zone 30	129
	5.2.6	Sub Zone 36-30	129
	5.2.7	Zone 40	131
	5.2.8	Zone 40-80	132
	5.2.9	Zone 50	134
	5.3	Natural Fracture Characterization (Verification Data)	136
	5.4	Quantitative Rxo in OBM in Marun Field	141
	5.5	RFT/MDT Survey Planning	144
	5.6	Reservoir Fluid Mobility	148
	5.7	Index Permeability from OBMI in MN-322	149
	5.7.1	Separations between HDRS, HMRS and OBMI-Rxo Curves	149
	5.7.2	Index Mobility in Marun-322	156
	5.8	Verification of OBMI Index Permeability with XPT Permeability	158
	5.9	The Evaluation of OBMI-UBI Result Comparing with Cores in Sarvak Fractured Reservoir (GS-016)	161
	5.9.1	OBMI-UBI Analysis	161
	5.10	Comparison between OBMI-UBI and Core Image	168
	5.10.1	Comparison of Results	169
	5.11	Summary	173
<b>6</b>		<b>BOREHOLE CONDITION EVALUATION BY USING FMI AND UBI</b>	<b>175</b>
	6.1	Introduction	175
	6.2	Detailed Borehole Shape Analysis	175
	6.2.1	Borehole Restrictions	184
	6.2.2	Optimization of Mud Weight	184
	6.2.3	Efficient Use of Lost Circulation Material	186
	6.2.4	Alteration to Well Trajectory	186
	6.3	Time Lapse Imaging	187

6.3.1	Borehole Stability	187
6.3.2	Fracture Characterization	188
6.3.3	Pressure and Fluid Sampling Points	189
6.3.4	Fluid Movement	189
6.4	Summary	191
<b>7</b>	<b>CONCLUSIONS</b>	<b>192</b>
7.1	Development of an Accurate Structural Model	192
7.2	Characterization of Fractured Reservoirs	193
7.3	Computation of Reliable Mobility Index	194
7.4	Evaluation of the Borehole Condition	195
	<b>REFERENCES</b>	<b>198</b>

## LIST OF TABLES

TABLE NO.	TITLE	PAGE
2.1	Significant events in the development of borehole imaging tools.	22
2.2	UBI specification (Schlumberger, 2002).	28
2.3	Applications of borehole images acquired with Schlumberger borehole imaging tools.	35
2.4	New applications of borehole images in the research study.	35
4.1	Summary of the characterization of fracture zones, mainly based on the mean porosity of the interval.	101
4.2	Zones of raw permeability index and secondary porosity.	107

## LIST OF FIGURES

FIGURE NO.	TITLE	PAGE
1.1	Studied oilfields (red colored) in Dezful embayment.	2
1.2	Asmari and Sarvak reservoirs in Iran (Bosold et al., 2005).	3
2.1	Asmari and Sarvak reservoirs in Iran (Schlumberger, 2005).	9
2.2	Geological and structural units of Iran (Richards et al., 2006).	11
2.3	Tectonics map showing location of Iran between the Eurasian and Arabian tectonic. Foreland folding in the south west of Zagros convergence and large-scale strike-slip faults are indicated in Iran (Motiei, 1995).	12
2.4	NW-SE trending major anticline structures in the Foreland basin of the Zagros Mountains (Motiei, 1995).	12
2.5	Normal, reverse and strike-slip faults (Costain and Coruh, 1989).	14
2.6	Increased borehole coverage over time. As more image data are acquired from around the circumference of the borehole, a more comprehensive interpretation is possible. Schlumberger micro resistivity-imaging devices have progressively added more sensors and pads to improve borehole coverage (Cheung and Laronga, 2001).	25
2.7	Schematic showing (a) side and (b) front views of a pad of OBMI. The tool has four pads; each pad carries five sets of sensors, which measure the voltage drop DV in the formation facing the sensors. To get more borehole coverage, more than two passes can be made that can be displayed together in one track (Cheung and Laronga, 2001).	25
2.8	Schematic showing (a) side and (b) front views of a pad of OBMI. An AC current is injected between the current electrodes A and B via the formation. Two voltage button sensors (C and D) measure the voltage drop V in the formation facing the sensors (Cheung and Laronga, 2001).	26
2.9	OBMI specification (Cheung and Laronga, 2001).	26
2.10	UBI tool Configuration and right, UBI transducers for different hole sizes (Cheung and Laronga, 2001).	27

2.11	Optimization of mud weight (Jeffreys, 2005).	30
2.12	Example of breakouts and drilling-induced fractures (DIFs) observed on acoustic image logs.	32
3.1	Specific research activity workflow.	37
3.2	Logging tools used to gather geological data.	39
3.3	Cross-plot between Ax & Ay, axes of accelerometers and FX & FY of magnetometers indicate that the directional information from GPIT is correct.	44
3.4	Flow chart of FMI and OBMI-UBI image processing chain.	45
3.5	Oriented enhanced image (right: before speed correction and left: after speed correction) (Schlumberger, 1999).	47
3.6	Static versus resistivity matched (Schlumberger, 1999).	48
3.7	Left: static image (Equalized) computed over the entire file, and right: Dynamic image (Enhanced) computed over 20 cm sliding window.	50
3.8	OBMI Static and Dynamic image in Marun-297.	52
3.9	Geoframe snapshot showing ultra-sonic image attributes editor panel.	54
3.10	Geoframe snapshot showing cross section plot (left) and spiral plot (right).	54
3.11	UBI Static and Dynamic image in Marun-297.	55
3.12	Basic of dip computation (Schlumberger, 1999).	57
3.13	Left, manual picking of points for dip computation, and right, calculated dip plane.	58
3.14	Different dips planes (Schlumberger, 1999).	58
3.15	FMI image showing layering within the Asmari formation. The dips corresponding to layer / bed boundaries are shown as high and low confidence based on their sharpness and planarity for computation of structural dip. Dips of high confidence bedding (circle green tadpoles) and low confidence bedding (triangular green tadpole) are presented in Asmari formation.	61
3.16	Example of open fractures and open vuggy fracture in Asmari formation seen by the FMI. The most of the open fractures are not continuous.	62
3.17	Example of closed fractures (resistive fractures).	63
3.18	Background conductivity and layer computation.	65
3.19	A snapshot from BorTex (software used to extract heterogeneities and layer details from images) highlighting the type of information output by itself. Displayed in the is a formation average background and layer conductivities in Track-3 and True-Stratigraphic-Thickness in Track-4.	66

3.20	A principle used in BorTex to identify spots and patches.	68
3.21	BorTex heterogeneity analysis of a FMI image. Note the fit between the vuggy zones in the carbonate of the core and the conductive anomalies (red spots) in the BorTex display.	69
3.22	FMI calibrated images highlighting resistive features comprising a section of Asmari Formation. Contoured / outlined in blue are resistive / dense features (patches in cyan and spots in blue (the spots are those dense / resistive features / areas whose dimensions are less than $0.003 \text{ m}^2$ )).	70
3.23	FMI calibrated images highlighting conductive features comprising a section of Asmari formation. Contoured/outlined in red are conductive-connected spots (i.e., the features smaller than $0.0003 \text{ m}^2$ ), in dark brown are isolated conductive spots, and in dark magenta are conductive patches (i.e. conductive features, larger than $0.003 \text{ m}^2$ ).	70
3.24	Formula for normalization of FMI permeability.	71
3.25	OBMI-UBI image showing layering within Asmari formation. The dips corresponding to layer/bed boundaries are shown as high and low confidence based on their sharpness and planarity for computation of structural dip.	72
3.26	Continuous (blue circular dips) and discontinuous (blue triangular dips), possible (blue minus dips) open fractures by OBMI-UBI image in Asmari formation.	73
3.27	Closed (cyan circular dips) fractures shown by OBMI images in Asmari formation.	74
3.28	Lamination density in Asmari reservoir in Marun-322.	76
4.1	The location map of the well#LL-26 in the Lali Field.	80
4.2	The location map of the well#PZ-126 in the Pazanan field.	80
4.3	Layering in Asmari formation and statistical plots of bedding dips indicating an average dip of 24 degrees S38W and strike N52W-S52E. Average dip inclination of 24 degrees is the most representative of the whole interval of Asmari formation.	82
4.4	Open fractures (blue circle) in Asmari are striking as oblique to the bedding strike.	83
4.5	Open fractures in Asmari striking as oblique to the bedding strike, Schmidt projection plot (upper hemisphere) of fracture dip poles. The dip inclination histogram shows large spread for a dip while dip azimuth rosette shows that the most of the fracture dips to the southwest with a large scatter.	84
4.6	Composite plot of orthogonal calipers (C1 and C2), GR, FMI static normalized images, dips, well deviation, FMI fractures, RHOZ, NPHI, PEFZ and resistivity curves in Asmari formation. Major fault is in zone 5 with dipping to the NNW at 59 degrees.	87

4.7	Composite plot of orthogonal calipers (C1 and C2), GR, FMI static normalized images, dips, well deviation, FMI fractures, RHOZ, NPHI, PEFZ and resistivity curves in Asmari formation. The combination of FMI and open hole logs (resistivity) shows major fault 1819m in zone 5 of Kalhur member.	88
4.8	Schematic computer generated model using the reverse-fault model (major fault in zone 5).	89
4.9	Composite plot of orthogonal calipers (C1 and C2), GR, FMI static normalized images, dips, well deviation in Asmari formation. Schematic computer generated model using the reverse-fault model. Drag zone and disturbed zone associated with the fault are shown. See over-turning of beds in the fault influenced zone. Structural dips of the sections above and below the faulted region are also marked.	89
4.10	The new sidetrack (red) is drilled based on the studied structural model in the sidetrack 1 (blue).	90
4.11	High confidence (circle green tadpoles) is presented in Gachsaran formation.	91
4.12	Statistical plots of bedding dips indicating an average dip of 26 degrees S36W and strike N54W-S54E. An average dip inclination of 26 degrees is the the most representative of the whole interval of Asmari formation.	92
4.13	Computer based structural cross-section using bedding dip data projected along SSW-NNE plane. A structural dip of 26 degrees S36W the most representative of the whole interval of Asmari formation.	93
4.14	Composite plot of orthogonal calipers (C1 and C2), HCGR, FMI static normalized images, dips, well deviation, open fracture density, aperture, porosity, resistivity curves, RHOZ,	95
4.15	Minor open fractures (blue triangle dips), Medium open fractures (blue circular dips) and Major open fractures (blue square dips) shown by FMI image in Zone 6.1 of Asmari formation.	98
4.16	Statistical plots for dips of all open fractures in the Asmari formation.	99
4.17	Statistical attribute dips of all fractures and bedding dip attribute showing commonly oblique fractures in the Asmari interval.	100
4.18	FMI calibrated images showing yellow lines (forming cluster of yellow lines) connecting the conductive spots (red contoured features) in a section of Asmari Formation.	103
4.19	Porosity histogram display over a section of Asmari (Sub Zone 2-1). In this zone, FMI has detected a higher porosity	

	streak and porous patches, which Log porosity is not responding and remains constant.	105
4.20	Composite plot of orthogonal calipers (C1 and C2), HCGR, FMI static normalized images, open fracture density, aperture, porosity, resistivity curves, PHIT, NPHI curves, MDT pressure, MDT mobility points, lithology, FMI image, porosity and FMI raw permeability indicator across the Asmari formation.	108
4.21	Good match between FMI and core permeability.	109
4.22	Porosity waveform histogram/secondary and total porosity from FMS, 3680-3682m. This interval is near the boundary of the layers 5 & 6. The rock texture is changed and porous/permeable sections are indicated by the image and Prospect*. The core sample photo is clearly showing a big vugs, which is also seen on the image.	111
4.23	Porosity waveform histogram/secondary and total porosity from FMS, 3682-3684m. This interval is one of the most productive intervals in the borehole. The slabbed core photo is clearly indicated vuggy section, which is distinctive on the image and from the results.	112
4.24	Permeability analysis results, Layer-6.	114
4.25	Composite plot of orthogonal calipers (C1 and C2), GR, FMI static normalized images, open fracture density , aperture, porosity, resistivity curves, PHI, TNPH curves, lithology, FMI image, FMI porosity and FMI raw permeability indicator across Asmari formation.	116
5.1	Location map of the well#MN-322 in the Marun field.	120
5.2	A section of Gachsaran contour map showing location of well GS-16.	120
5.3	Header details for 5.4.	122
5.4	High and low confidence OBMI and UBI bedding in Asmari formation.	123
5.5	Marun reservoir zonations (N.I.S.O.C et al., 2003)	124
5.6	Lithology and statistical plots for dips of Zone 1 bed boundaries.	125
5.7	Lithology and statistical plots for dips of zone 11.	126
5.8	Lithology and statistical plots for dips of Zone 20 bed boundaries.	127
5.9	Lithology and statistical plots for dips of sub Zone 28 bed boundaries.	128
5.10	Lithology and statistical plots for dips of Zone 30 bed boundaries.	130



5.11	Lithology and statistical plots for dips of Zone 36-30 bed boundaries.	131
5.12	Lithology and statistical plots for dips of Zone 40 bed boundaries.	132
5.13	Lithology and statistical plots for dips of Zone 40-80 bed boundaries.	133
5.14	Lithology and statistical plots for dips of Zone 50 bed boundaries.	134
5.15	Statistical plots of bedding dips indicating an average dip of 35 degrees N32E and strike N58W-S58E. Average dip inclination of 35 degrees is the most representative of the whole interval of Asmari formation.	135
5.16	Computer based structural cross-section using bedding dip data projected along SSW-NNE plane. A structural dip of 37 degrees S45W is the most representative of the whole interval of Asmari formation.	136
5.17	Continuous (blue circular dips), discontinuous (blue triangular dips) open fractures shown by UBI and OBMI images in Asmari formation.	138
5.18	Statistical plots of dips of all open fractures in the Asmari interval.	139
5.19	Statistical plots of dip attributes of all closed fractures in the zones of Asmari formation.	139
5.20	Composite plot of GR, orthogonal calipers (C1 and C2), RHOB, NPHI and PE curves, resistivity curves, XPT pressure data on the OBMI image, OBMI static normalized images, dips, OBMI-UBI open and closed fracture, well deviation, UBI static normalized images and lithology.	140
5.21	A section of the Marun contour map showing location of well MN-292.	141
5.22	OBMI Rxo showing large separation from induction resistivity logs in a section of Asmari sandstone sections of the MN-292 of Marun field.	142
5.23	OBMI Rxo display separation from induction resistivity logs in carbonate.	143
5.24	Large separation between OBMI Rxo and induction resistivity logs in a section of Asmari sandstone sections of the MN-292 of Marun field.	143
5.25	OBMI Rxo showing large separation from induction resistivity logs in a section of Asmari sandstone sections of the well MN-292 in Marun field indicating large invasion due to permeability. RFT mobility (blue circles) also computes higher mobility in the same sections.	145

5.26	The location of dry test points (yellow circles) of RFT in a section of Asmari of well MN-292 of Marun field, correspond to shale streaks or very low permeability streaks indicated by OBMI images. No invasion in such streaks is observed on Rxo and induction curves indicating their very low permeability. RFT formation mobility is indicated by blue circles.	145
5.27	A section of Marun contour map showing location of well MN-297	146
5.28	The locations of dry test points (yellow circles) of RFT in a section of Asmari, correspond to shale streaks or very low permeability streaks indicated by OBMI images. No invasion in such streaks is observed on Rxo and induction curves indicating their very low permeability. RFT formation mobility is indicated by blue circles.	147
5.29	Locations of dry test points (yellow circles) of RFT in a section of Asmari of well MN-297. RFT formation mobility is shown by blue circles.	149
5.30	The separation between OBMI Rxo and HDRS, HMRS (deep and shallow resistivity) shows high mobility zones comparing with XPT mobility (yellow circle) in the water zone.	150
5.31	The separation between OBMI Rxo and HDRS, HMRS (deep and shallow resistivity) shows high mobility zones comparing with XPT mobility (yellow circle) in the oil zone.	151
5.32	The separation between OBMI Rxo and HDRS, HMRS (deep and shallow resistivity) show oil based mud fluid invasion because of borehole damage	152
5.33	The separation between OBMI Rxo and HDRS, HMRS (deep and shallow resistivity) is an indication of no invasion comparing with XPT mobility (yellow circle).	153
5.34	OBMI Rxo shows borehole damage in zones of high formation resistivity.	154
5.35	Match between OBMI Rxo and HDRS, HMRS (deep and shallow resistivity) shows no invasion and impermeable formation oil saturated rock with very irreducible water.	155
5.36	Composite plot of GR, orthogonal calipers (C1 and C2), RHOB and NPHI curves, OBMI static normalized images, XPT pressure data, dips, well deviation, UBI static normalized images, lithology, and Index mobility from OBMI in the Asmari reservoir.	157
5.37	XPT mobility in different depth interval in Asmari reservoir.	158
5.38	Composite plot of GR, orthogonal calipers (C1 and C2), RHOB and NPHI curves, OBMI static normalized images, XPT pressure data, dips, well deviation, UBI static normalized images, lithology, index mobility from OBMI, index	

	permeability from OBMI and XPT (red circle) in the Asmari reservoir.	160
5.39	OBMI and UBI images showing layering due to argillaceous intercalations within upper Sarvak. The dips corresponding to layer/bed boundaries are shown as low and high confidence based on their sharpness and planarity for computation of structural dip.	163
5.40	Statistical plots of all bedding dips indicating a dominant structural dip of 71 degrees S38W and strike N52W-S52E.	164
5.41	Computer based structural cross-section using bedding dip data projected along a NNE-SSW plane.	165
5.42	A highly fractured section in the middle part of the reservoir, showing continuous and discontinuous open fractures.	167
5.43	The summary of fracture analysis results in GS-16. Apart from some short sections open fractures are present in its most intervals.	170
5.44	Clear bedding planes dipping 50-60 degree SW along with minor open fractures (partially cemented).	171
5.45	Interval where UBI images affected by borehole breakout whereas OBMI images clearly indicate the bedding planes and minor fractures (probably cemented).	171
5.46	Major open fracture cross- cutting bedding plane possible slickenside on core along the fracture plane.	172
5.47	The clear example of both major and minor fracture types on OBM log images coinciding with broken core.	172
5.48	Image log shows intensive fracturing hence the core rubble.	173
6.1	Fracture patterns examples of UBI cross-section plots in Iran.	177
6.2	Borehole breakouts and hydraulic fractures indicate that orientation of the maximum horizontal stress is changing across the studied field.	179
6.3	In-Situ stress analysis provided in different wells in the Marun field (Movahed et al., 2014).	180
6.4	In-Situ stress analysis provided in different wells in Gachsaran field (Movahed et al., 2014).	180
6.5	Image logs quality control flag color.	182
6.6	UBI image of the borehole radius showing borehole enlargements (breakouts – black vertical stripes) around NW and SE sides of the borehole.	185
6.7	Asymmetrical borehole wall damage resulting from mechanical wearing related to reaming and pipe rotation.	187














6.8	FMI Images acquired over a period of 7 days, the increase in aperture of drilling fractures and the development and/or enlargement of borehole breakouts (left to right).	190
-----	---	-----

## LIST OF ABBREVIATION

<i>BS</i>	-	Bit Size
<i>C1</i>	-	Caliper Pair 1-3
<i>C2</i>	-	Caliper Pair 2-4
<i>CGR</i>	-	Gamma Ray (Corrected)
<i>CKH</i>	-	Core Horizontal Permeability
<i>COND.CONNECTED.SP</i>	-	Conductive Connected Spots
<i>COND.PATCHES</i>	-	Conductive Patches
<i>COND.ISOLATED.SPOT</i>	-	Conductive Isolated Spots
<i>CPOR</i>	-	Core Porosity
<i>CS</i>	-	Cable Speed
<i>DEVI</i>	-	Borehole Deviation Angle (deg)
<i>DYNAMIC</i>	-	Sliding Window Normalization
<i>EMEX</i>	-	Measurement Control Voltage
<i>FMI</i>	-	Full bore Formation Micro Imager Tool
<i>FRACTURE APERTURE</i>	-	Aperture of Fractures
<i>FRACTURE DENSITY</i>	-	Number of Fractures Per Meter
<i>FRACTURE POROSITY</i>	-	Porosity of Fractures
<i>GEOLOG</i>	-	Geological Lithozones
<i>GPIT</i>	-	General Purpose Inclinometry Tool
<i>HAZI</i>	-	Borehole Deviation Azimuth (deg)
<i>HC BEDDING</i>	-	High Confidence Bedding
<i>HDRS</i>	-	Deep Resistivity
<i>HGR</i>	-	Gamma Ray
<i>HMRS</i>	-	Shallow Resistivity
<i>ILD</i>	-	Deep Resistivity (Deep Induction)
<i>ILM</i>	-	Shallow Resistivity (Shallow Induction)
<i>LQC</i>	-	Log Quality Control

<i>LC BEDDING</i>	- Low Confidence Bedding
<i>MDT</i>	- Modular Formation Dynamics Tester Tool
<i>NPHI</i>	- Neutron Porosity
<i>OBMI</i>	- Oil Base Mud Imager
<i>P1AZI</i>	- Pad 1 Azimuth (deg)
<i>PE</i>	- Photoelectric Factor
<i>PEFZ</i>	- Photoelectric Factor
<i>PERM</i>	- Permeability from FMS
<i>PERM.INDEX</i>	- Raw FMI Permeability Indicator (Mobility)
<i>PEX</i>	- Platform Express
<i>PHIS</i>	- Secondary Porosity
<i>PHIT_FMI</i>	- Average High-resolution Porosity from FMI
<i>PIGE</i>	- Shale Corrected Log Porosity
<i>POR_HIST</i>	- Porosity Histogram
<i>PP</i>	- Pad Pressure
<i>RES.SOPTS</i>	- Resistive Spots
<i>PES.PATCHES</i>	- Resistive Patches
<i>RHOZ</i>	- Formation Density
<i>RLA3</i>	- Shallow Resistivity
<i>RLA5</i>	- Deep Resistivity
<i>SPOR</i>	- Secondary Porosity from FMI
<i>STATIC</i>	- Fixed Window Normalization
<i>TENS</i>	- Tension
<i>TNPH</i>	- Porosity from Neutron Log
<i>UBI</i>	- Ultrasonic Borehole Imager tool
<i>WALL</i>	- Borehole Wall
<i>XPT</i>	- Xpress Pressure Tool

## LIST OF SYMBOLS

Symbol		Dip Classification
	-	High Confidence Bedding
	-	Low Confidence Bedding
	-	High Confidence OBMI Bedding
	-	Low Confidence OBMI Bedding
	-	High Confidence UBI Bedding
	-	Low Confidence UBI Bedding
	-	Minor Open fractures
	-	Major open fractures
	-	Medium open fractures
	-	Closed fracture
	-	Continuous open fractures
	-	Discontinuous open fractures
	-	Fault

## **CHAPTER 1**

### **INTRODUCTION**

#### **1.1 Introduction**

Outcrop study of the target formations/ reservoirs have a great importance to understand the possible geological (structural and sedimentological) and reservoir characteristics of the reservoir. These features are studied at different scales to determine their lateral and vertical extent and distribution. This is mainly achieved by various technologies, such as, Brunton compasses/Inclinometers, topographic maps, aerial photographs, and satellite images. A similar approach is needed for delineating and characterizing the reservoirs in the subsurface. The large scale subsurface features are delineated with the surface seismic (2D and 3D) techniques. However, the coarse resolution (generally greater than 10 m) of these techniques does not allow for feature identification of smaller scales (for instance, cross bedding, bedding, fractures, and vugs/moulds) that are very useful for detailed characterization of reservoir rocks.

Borehole images are very useful in cases where information on geological (structural and sedimentological) and reservoir features are required. Structural dip by definition is the present day formation dip used to build the structural cross section. It is also a record of the post-depositional structural alteration and may indicate the tectonic history of the sequence. It is not an average dip for all the bedding planes. Apart from structural analysis, the investigation of fractures is the main application for image logs in Dezful Embayment, Iran. Information on fractures is important to know because of their higher permeability, hence their



biggest influence on reservoir producibility. Schlumberger provides high quality borehole images in wells drilled with all types of mud; water based mud and oil based mud. These images can be acquired in wells of all geometries ranging in deviation from 0.0 degrees to more than 90 degrees. It is now possible to get resistivity of the invaded zone ( $R_{xo}$ ) in the wells drilled with oil-base mud using the state-of-the-art imaging tool called the Oil Base Mud Imager (OBMI) (Schlumberger, 2005). By using advanced interpretation, it can compute permeability from the borehole images in carbonates.

This study highlights the importance of data integration and borehole images in the domains of geology, petrophysics, geomechanics/drilling, reservoir and production engineering in different oil fields of National Iranian South Oil Company (NISOC). Borehole images logged in Asmari and Sarvak reservoirs from the NISOC fields like Lali, Gachsaran, Marun, Mansuri and Pazanan are discussed (Figure 1.1).

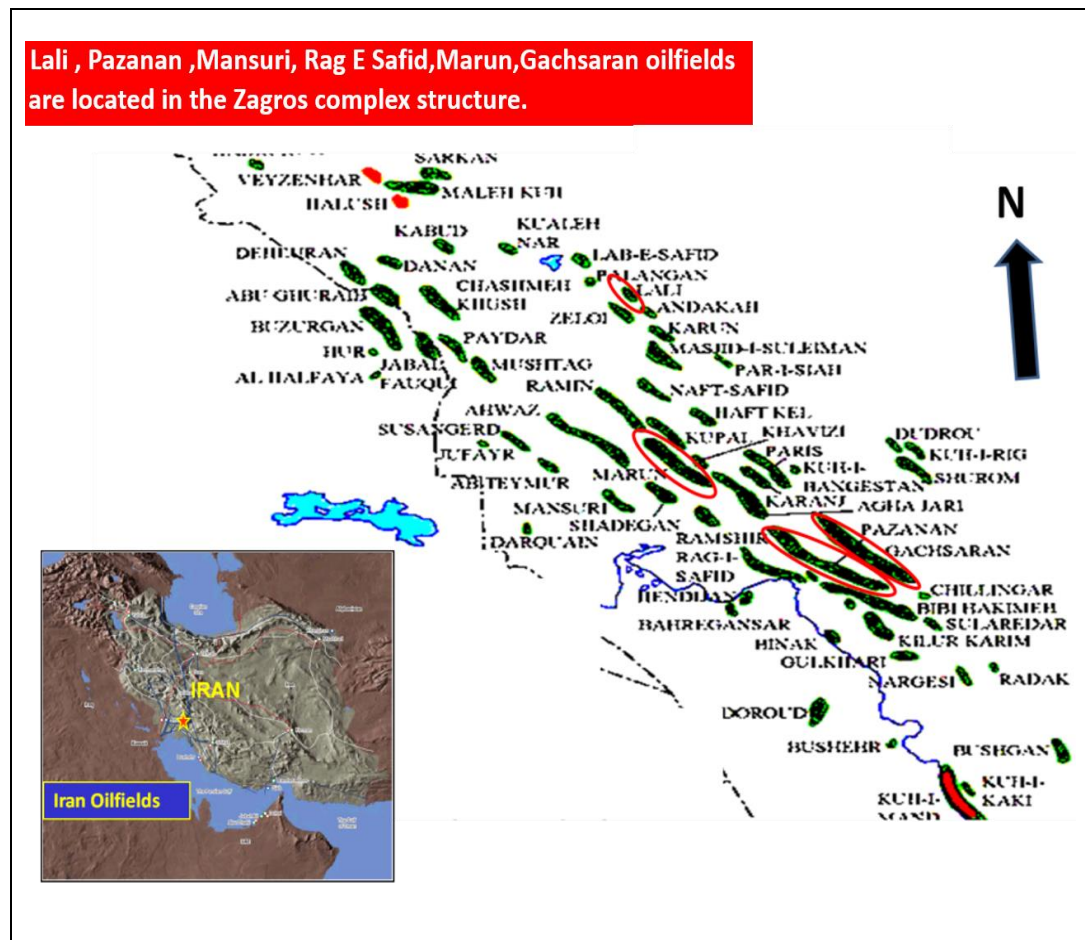


**Figure 1.1** Studied oilfields (red colored) in Dezful embayment.

The Asmari formation consists of limestones, dolomitic limestone, argillaceous limestone, and anhydrite and the lithology of Sarvak formation is limestone and it lies below Ilam reservoir (Motiei, 1993) (Figure 1.2). Our research establishes a technique to increase the reservoir explanation of the Asmari and Sarvak reservoir by using a new application of image logs.

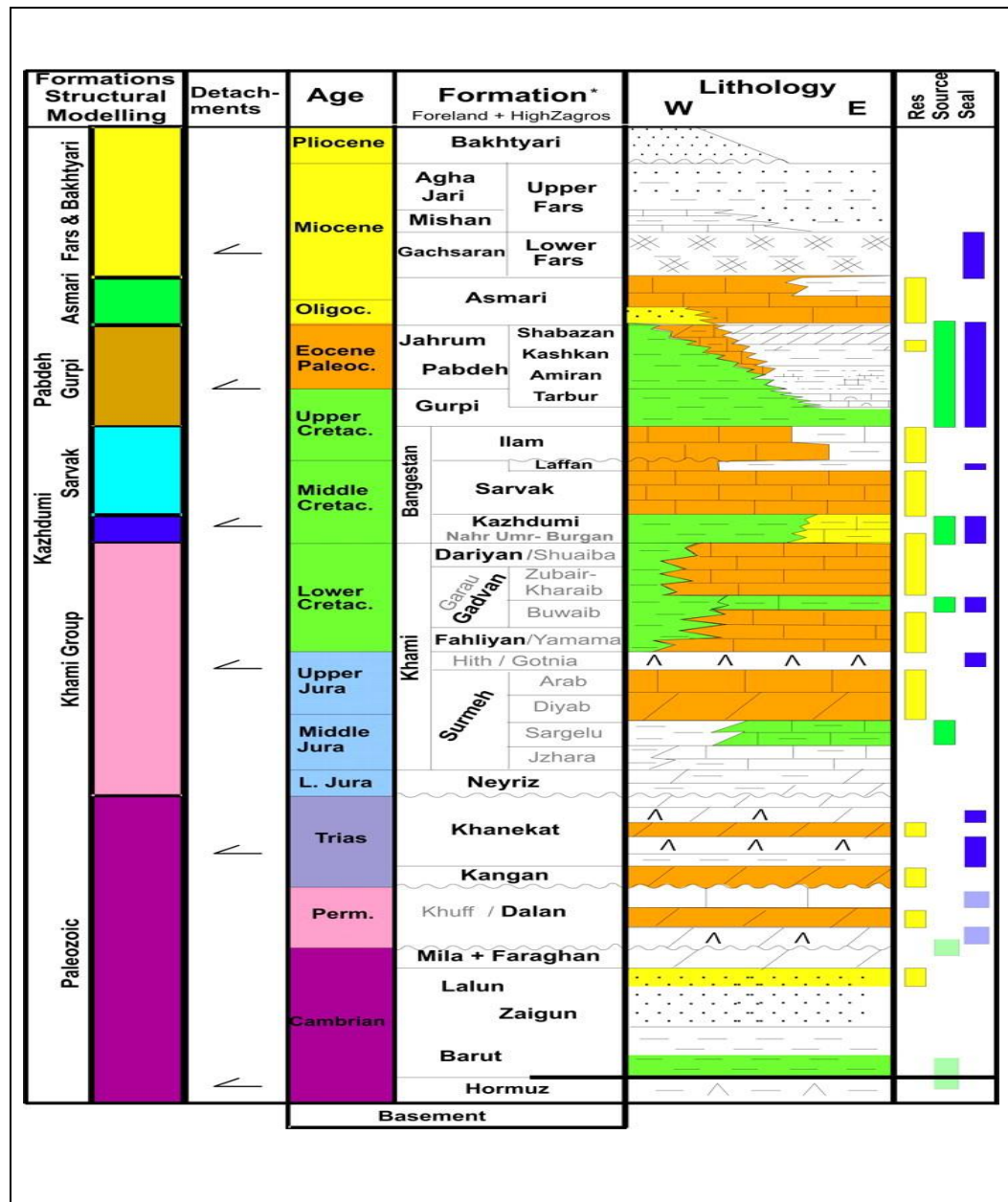


Figure 1.2 Asmari and Sarvak reservoirs in Iran (Bosold et al., 2005).

## 1.2 Problem Statement

The crossing Asmari reservoir is not so easy in some cases due to structural complexities, where there is a thick pile of evaporates of Gachsaran formation over the reservoir. In some wells, higher than the expected thickness of formations is found. Dip classification based on a geological log has the advantage of providing a direct representation of structural origin and identify Asmari fault and fracture systems and its influence on production and resolve structural complexity.

Fracture intensity and deep rooted fractures extensively increase risk of unexpected water production. So, it is vital to know, whether reservoir is fractured or not. If it is fractured then what is the kind of fractures (open or closed) and what is their intensity? Do they occur as a single set or multiple sets and what orientation is their dominant strike? Solutions to questions like these support geologists and reservoir engineers increase oil production (Movahed et al., 2014) and in this study the borehole imaging tools, like the Formation Micro Imager (FMI), Oil Base Mud Imager - Ultrasonic Borehole Imager (OBMI-UBI) are interpreted to find solutions for fracture systems and fracture attributes.

Permeability analysis of dual porosity systems with heterogeneous distribution of dissolution fabrics can evaluate by using the FMI, but NISOC is not using permeability from FMI in a case when there are no any formation testing data in the well for fracture and reservoir modeling. In this study, image logs provided the most representative measurements in geological and petrophysical heterogeneous formations and present a method to measure permeability from FMI in Asmari and Sarvak reservoirs.

OBMI-Rxo is a high resolution curve that is sensitive to fluid mobility near to the borehole wall and which indicates invasion and indirectly lithology, but NISOC is not using an accurate Rxo curve of OBMI for reservoir and petrophysical application. This method using resistivity classes is used to show how the high resolution OBMI curves can be used. The result of this research demonstrates the

new analytical method to evaluate a fractured carbonate and clastic reservoirs from Iran.

The most wells drilled in Iran suffer from geomechanical hazards owing to the high in-situ stress related to the proximity of the Zagros Mountain and it is not always possible to acquire wireline log data because of the borehole condition (Movahed et al., 2014). In this study, advanced borehole shape analysis by using FMI and UBI helped regarding borehole instability and improved information about the well condition.

### **1.3 Objectives of the Research**

The objectives of the research are given below:

1. To develop an accurate structural model for Asmari reservoir.
2. To characterize fractures in the borehole.
3. To compute reliable index mobility from OBMI and index permeability from FMI.
4. To evaluate the borehole condition in order to reduce drilling risk and avoid potential well bore damages.

### **1.4 Scopes of the Research**

Borehole images were integrated with other data (petrophysical, reservoir, and geophysical) to understand the various characteristics of the Asmari both in oil based mud and water based mud systems. In this study, borehole images are used to solve different issues in geology, petrophysics, reservoir engineering, production engineering, sedimentology, geomechanic and drilling in NISOC oil fields that is explained in the following:

1. Image log data are processed for a number of factors that may affect the quality of the images in Geoframe. Such factors include: variation in speed of the tool relative to the drill-pipes, or cable speed; sticking of the tool. Additionally, image logs are equalized and normalized to improve the information of features in it. Interpretation typically started with hand picking dips using sinusoid techniques on image log presented at 1:20 or 1:10 scale so that the geological features are easily visualized. Once dips have been picked they have to be classified into bed boundaries and fractures.
2. Interpreting structural dip resolved structural complexity, thus provided the exact location of the well in the Asmari reservoir, which could not reach the lower contact of Asmari by interpreting FMI images and petrophysical logs in wells LL-26.
3. The structural dip from PZ-126 was used as input for permeability analysis and it was imported into the Bortex module and computed reservoir heterogeneity from FMI used to extract heterogeneities and layer details from images. In addition to formation heterogeneities, the software also calculated index permeability of the reservoir. Fracture properties (open or closed), occurrence, orientation, spacing, and porosity were interpreted by using Image log and imported as indirect input for permeability analysis.
4. The OBMI structural dip data is imported into the Bortex software in the MN-322.OBMI tool was used to identify zones of higher permeability when combined with conventional induction logs and porosity logs. Separation between Rxo curves (one from each of four OBMI pads) and induction logs, due to invasion of oil in the mud, indicated higher permeability.
5. The borehole cross sections are interpreted to give a very detailed account of the in-situ stress conditions by using UBI.

## REFERENCES

- Aadnoy, B. and Bell, S. (1998). Classification of Drilling-Induced Fractures and Their Relationship to In-Situ Stress Directions. *The Log Analyst*, v. 39, no. 6, November-December, pp. 27-42.
- Akbar, M. (1993). Finding Fractures in Tight Reservoirs. Schlumberger.
- Akbar, M., Petricola, M., and Watfa, M. (1994). Classic Interpretation Problems: Evaluating Carbonates. *Oilfield Review*, Vol. 7, no. 1, pp. 38-57.
- Akbar, M. and Sapru, A. (1994). In-Situ Stresses in the Subsurface of Arabian Peninsula and their Effect on Fracture Morphology and Permeability. 6th ADIPEC, ADSPE 99, Abu Dhabi, U.A.E.
- Akbar, M. , Petricola, M., Watfa, M., Badri, M., Charara, M., Boyd, A., Cassell, B. (2001). Porosity Analysis from FMI, Schlumberger.
- Alavi, M. (2004). Regional Stratigraphy of the Zagros Fold-thrust belt of Iran. *American Journal of Science*, Vol.304, pp. 1-20.
- Bell J.S. (1990). Investigating Stress Regimes in Sedimentary Basins Using Information from Oil Industry Wireline Logs and Drilling Records. *Geological Applications of Wireline Logs*, Geological Society Special Publication No. 48, London, pp. 305-325.
- Borbas, T., Wendt, B., Jacques, R., Tabanou, J.R., Cheung, P., Liu, C. B., Hansen, S., Lavigne, J., Omeragic, D. and Pickens, T. (2002). Thinly Laminated Reservoir Evaluation in Oil-Base Mud: High Resolution Versus Bulk Anisotropy Measurement, a Comprehensive Evaluation. SPWLA 43rd Annual Logging Symposium. 2-5 June. Paris, France.
- Bosold, A., Schwarzhans, W., Julapour, A., Ashrafzadeh, A.R. and Ehsani, S.M. (2005). The structural geology of the High Central Zagros revisited (Iran), RWE Dea AG, Ueberseering 40, D-22297 Hamburg.
- Bram, K., Harjes, H. P., Dürbaum, H. J., Gebrande, H., Gebrande, H., Hirschmann, G. , Janik, M., Klöckner, M., Lüschen, E., Rabbel, W., Simon, M., Thomas,

- R., Tormann, J., and Wenzel, F. (1995). Origin and Nature of Crystal Reflections. Results from Integrated Seismic Measurements at the KTB Superdeep Drilling Site.
- Bratton, T., Canh, DV., Van Que, N., Duc, NV., and Gillespie, P. (2006). Naturally Fractured Reservoirs, Oilfield, Schlumberger.
- Cheung, P., and Laronga, R. (2001). Field Test Results of a New Oil-Based Mud Formation Imager Tool. Transaction of the SPWLA 42nd annual logging symposium, Houston, Texas.
- Cheung, P. , and Laronga, R. (2002). Oilfield Review. Schlumberger.
- Costain, J. K., and Çoruh, C. (1989). Tectonic Setting of Triassic half-grabens in the Appalachians. Seismic data acquisition, processing, and results: American Association of Petroleum Geologists Memoir 46, p. 155-174.
- Cox, J. W. (1983). Long-Axis Orientation in Elongated Boreholes and its Correlation with Rock Stress data. Transactions of the SPWLA 24th Annual Logging Symposium, Calgary, Canada.
- Dauod, M. (2010). Advanced Field Scale Modeling. Schlumberger.
- Daungkaew S., Fujisawa, G., Chokthanyawat, S., Comrie-Smith, N., and Thaitong, T. (2012). Is there a better way to determine the viscosity in waxy crudes? SPE Asia Pacific Oil and Gas Conference and Exhibition, APOGCE.
- Haller, D., and Porturas, F. (1998). How to Characterize Fractures in Reservoirs Using Borehole and Core Images. Case Studies. Geological society, vol. 136. Special Publications, London, pp. 249 259.
- Jacques, W. (2010). The Handbook of Groundwater Engineering, Second Edition. Taylor & Francis. p. 7 in chapter 2. ISBN 978-0-8493-4316-2.
- Jeffreys, P. (2005). Hole shape and In-situ stress from Geological Images from Iran. Schlumberger
- Khoshbakht. F., Memarian, H., and Mohammadnia, M. (2009). Comparison of Asmari, Pabdeh and Gurpi formation's fractures derived from image log. Journal of Petroleum Science and Engineering 65 -74.
- Lehne, K.A. and Aadnoy, B. (1992). Quantitative Analysis of Stress Regimes and Fractures of Logs and Drilling Records of a North Sea Chalk Field. The Log Analyst, pp. 351-361.
- Ma, T. A. (1993). Natural and Induced fracture, classification using image analysis. Viewed 8 of February 2012 <[www.onepetro.org](http://www.onepetro.org)>

- Mitra, S. (2002). Fold Accommodation Faults. AAPG Bulletin, v. 86, no. 4, pp. 671-693.
- Motiei, H. (1993). Stratigraphy of Zagros in Hushmandzadeh. Treatise on the Geology of Iran: Tehran, Geological Survey of Iran, 536 p.
- Motiei, H. (1995). Petroleum Geology of Zagros. Geological Survey of Iran with cooperation of Deputy Ministry of project and planning, no. 25.
- Movahed, Z., Junin, R., Safarkhanlou, Z., and Akbar, M. (2014). Formation Evaluation in Dezful Embayment of Iran using oil-based-mud Imaging Techniques, Journal of Petroleum Science and Engineering 121 (2014) 23–37.
- Movahed, Z., Junin, R., and Jeffreys, P. (2014). Evaluate the Borehole Condition to Reduce Drilling Risk and Avoid Potential Well bore Damages by using Image Logs, Journal of Petroleum Science and Engineering 122 (2014) 318-330.
- Mount, V.S. and Suppe, J. (1987). State of Stress near the San Andreas Fault: Implications for Wrench Tectonics. Geology, 15, pp. 1143-1146.
- Nimmagadda, Shastri, Dreher and Heinz (2010). Ontology based Warehouse Modeling of Fractured Reservoir Ecosystems For an Effective Borehole and Petroleum Production Management. P 490 - 496
- N.I.S.O.C, Statoil and RIPI (2003). Sedimentology and Stratigraphy and Reservoir Quality of the Asmari formation in the Marun field.
- Nelson, R. A. (2001). Geologic Analysis of Naturally Fractured Reservoirs. Houston, Texas: Gulf publishing company. Pp. 322.
- Newberry, B. M., Grace, L. M. and Stief, D. (1996). Analysis of Carbonate Dual Porosity Systems from Borehole Electrical Images.
- Park, R. G. (2005). Foundation of Structural Geology (reprint of the 1997 Chapman and Hall edition) Routledge, Abingdon, England, page 9, ISBN 978-0-7487-5802-9.
- Prensky, S. E. (1999). Advanced in Borehole Imaging technology application.
- Rezaeei, M.R. (2006). The book of petroleum Geology, alavi propagation; 472p.
- Richards, J., Wilkinson, D. and Ullrich, T. (2006). Geology of the Sari Gunay Epithermal Gold, Department of Earth and Atmospheric Sciences, doi: 10.2113/gsecongeo. 101.8.1455 *Economic Geology* December 2006 vol. 101 no. 8 1455-1496



- Russell, S. D., Akbar, M., Vissapragada, B. and Walkden, G. (2002). Rock types and permeability prediction from dip meter and image logs. AAPG Bulletin, 86 (10), 1709-1732.
- Sadler, R (2002). Integrated characterization of fractures and faults of the Shu'aiba reservoir, Shaybah field, AJGS, v. 7, no. 2, p. 291-292.
- Sahin, A. and Ali, A. Z. (2011). Comparison of patterns of permeability anisotropy distributions in Jurassic and Cretaceous carbonate reservoirs, AJGS, v. 16, no. 2, p. 209-210.
- Schlumberger (1999). Borehole Image Measurements. Schlumberger documents.
- Schlumberger (2002). UBI- Advanced borehole imaging independent of mud type, SMP-5871.
- Schlumberger (2005). Stratigraphy and Geology of Iran, Reservoir Symposium.
- Sembiring, P., Bashir, N., and Danardatu, H. (2005). Oil Based Mud Micro Imager (OBMI) Application in Sangatta Field. SPE-92779-MS, SPE Asia Pacific Oil and Gas Conference and Exhibition, 5-7 April.
- Sepehr, M. (2004). The Structural Framework of the Zagros Fold–Thrust Belt, Iran, DOI: 10.1016/j. marpetgeo.
- Shang, R. , Tang, D. (2005). Fracture Pattern and Associated Aperture Distribution: Example from The Foothills, SPWLA, Paper AA.
- Shariatnia, Z., Haghighi, M. ,Feiznia, S., Hall, D., Levresse, G.,Dehghani, A. , and Rashidi, M. (2013). Paleofluid analysis from fracture-fill cements in the Asmari limestones of the Kuh-I-Mond field, SW Zagros, Iran, Arabian Journal of Geosciences, 2013: 6 (7):2539-2556, Springer, ISSN: 1866-7511.
- Shawky, I. (2006). Application of Most Recent Borehole Geophysical Logging for Aquifer Characterization, Proceedings of the 5th International Symposium on Management of Aquifer Recharge, Berlin, Germany, 11-16 June 2005, UNESCO, Paris, p. 467-473.
- Soliman, Osama M., Saad Aba, A.,and Bader, A. (2010). Tectonic and Climatic Controls of Post Glacial Terminal Fluvial Systems, Permian Unayzah Reservoir.
- Sorkhabi, R. (2014). How Much Oil in the Middle East? Vol. 11, No. 1 – 2014.
- Stocklin, J. (1968). Structural History and Tectonics of Iran. AAPG, Bull.52, pp. 509-526.

- Stroble, R. (2009). The Value of Dipmeter and Borehole Images in oil sands Deposit. A Canadian Study.
- Szabo, F. and Kheradpir, A. (1978). Permian and Triassic stratigraphy, Zagros Basin, South West Iran. *Journal of Petroleum Geology*, 1,2, pp. 57-82.
- Tatar, M., Hatzfeld, D., and Ghafory-Ashtiany, M. (2004). Tectonics of the Central Zagros (Iran) deduced from micro-earthquake seismicity, *Geophysical Journal International*, v. 156, pp. 255-266.
- Tingay, M., Reinecker, J., and Müller, B. (2008). Borehole Breakout and Drilling-Induced Fracture Analysis of Image Logs, World Stress Map Project.
- Watts, N.L. (1983). Microfractures in Chalks of Albuskell Field, Norwegian sector, North Sea, possible origin and distribution, *AAPG bulletin*, v. 67, No. 2, p 201-234.
- Wazeer, F., Ismail, F., and Standen, E. (1990). Fracture Geometry and Hydrocarbon Productivity in the Basement Rocks of the Zeit Bay Field - Gulf of Suez, Egypt, EGPC exploration and Production Conferencing.
- Yang, J., Gou, X., Hilmi, N., and Xia, R. (2012). Identify Fracture Features and to Classify Fracture Types. *Fractured carbonate reservoirs*.
- Zhang, J. (2013). Borehole Stability Analysis, Accounting for Anisotropies in Drilling to Weak Bedding Planes. *Int. J. Rock Mech. Min. SCI.* 60,160-170.